CHAPTER 4

Results and Discussion (Part I): Indium Tin Oxide (ITO) Films

Deposition and properties of the effects of Sn doping on In_2O_3 films are investigated in this chapter. These films were deposited by the ultrasonic spray pyrolysis technique and the properties such as thickness, crystal structure, morphology, optical properties and electrical properties were measured.

4.1 Film preparation

4.1.1 Starting solution preparation

The starting solutions for ITO films were prepared from indium chloride ($InCl_3$) and tin chloride ($SnCl_4 \cdot 5H_2O$) as dopant, which were dissolved in ethanol (C_2H_5OH) and deionized water (DI water) in the volume ratio of 1:4. Hydrochloric (HCl) acid was added to increase the solubility. The compositions of these solutions were a fixed 0.025 M of $InCl_3$ while the atomic percentage ratio of Sn/In was varied from 0 to 9 at.%, as listed in Table 4.1.

Table 4.1 Specifications of materials and compositions of the starting solutions for ITO films used in this study.

Materials	Source	Purity	Solution compositions
$InCl_3$	Sigma-Aldrich	99.999%	0.025 M
$SnCl_4 \cdot 5H_2O$	Sigma-Aldrich	≥98%	0-9 at.% Sn
C_2H_5OH	EMSURE®	absolute	20 % of solution
DI water	-	-	80 % of solution
HCl	EMSURE®	37%	0.05 M

4.1.2 Spray coating

All starting solutions were sprayed on microscope glass substrates heated at 350°C by using ultrasonic spray pyrolysis in air. The distance between the nozzle and the substrate was 20 cm with nozzle frequency of 34 kHz and spray rate of 2.5 ml/min for a total time of 3 min. The samples after coating were annealed in an electric furnace at 500°C for 1 hour using a heating/cooling rate of 5°C/min. The schematic diagram of the ITO film fabrication process is shown in Figure 4.1.

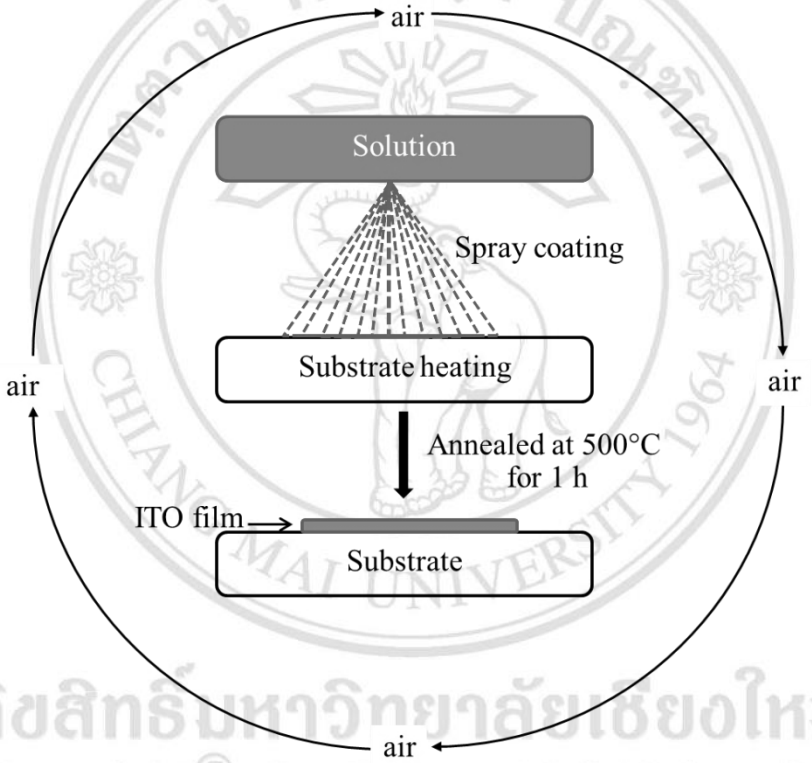

Figure 4.1 Schematic diagram of ITO film preparation.

4.2 Results and discussion

Images of ITO films with different Sn concentrations deposited on glass substrates are shown in Table 4.2. It was found that all films had high transparency. The characterizations of these films such as thickness, crystal structure, morphology optical and electrical properties are described in the following sections.

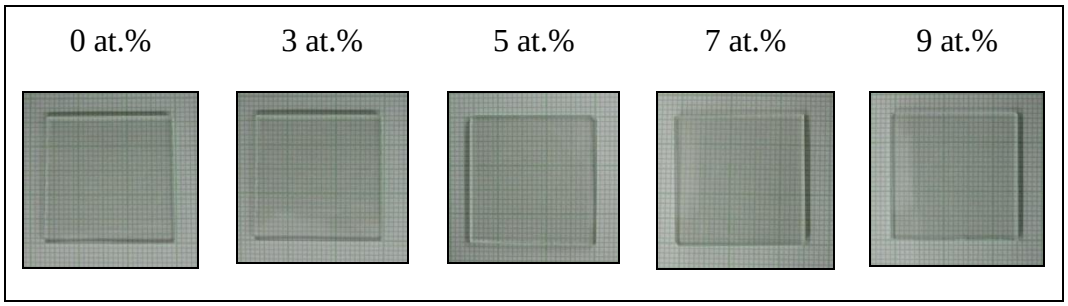

Figure 4.2 Images of ITO films with different Sn concentrations deposited on glass substrates.

4.2.1 Thickness

Figure 4.3 shows the SEM cross section microstructures of ITO films with different Sn concentrations deposited on glass substrates. It was observed that the films grew well on the glass substrate.

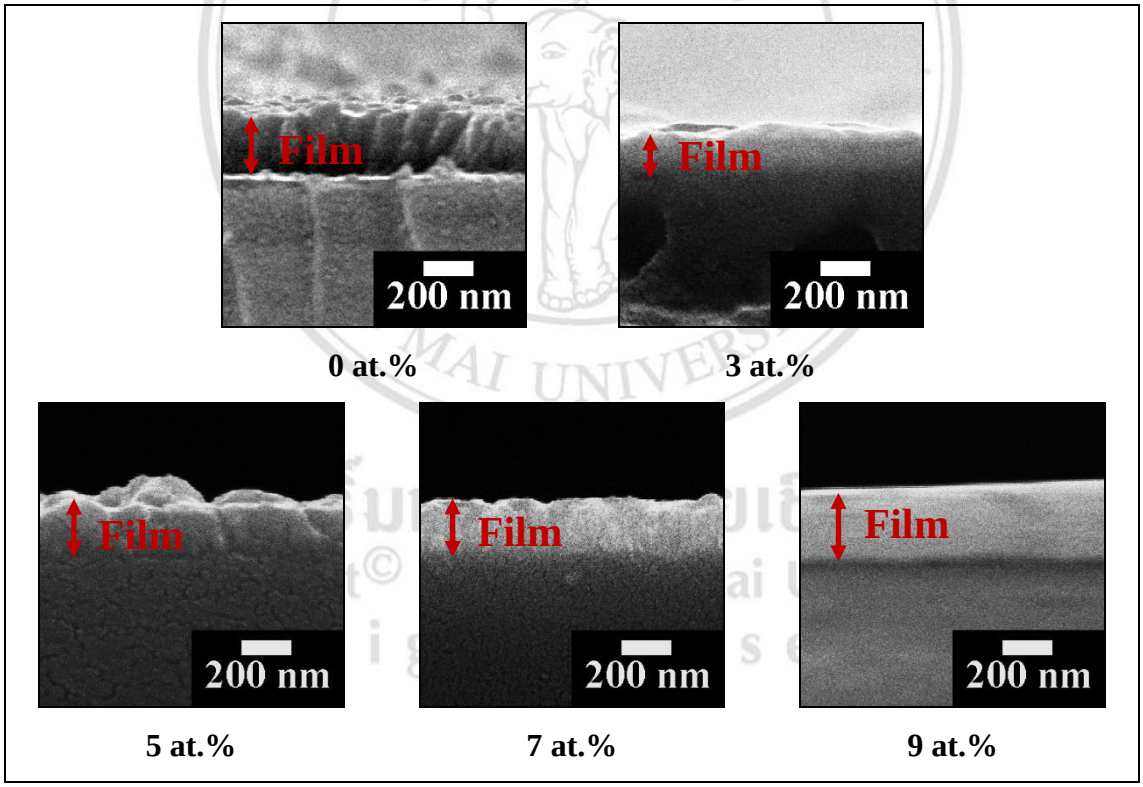

Figure 4.3 SEM cross section microstructures of ITO films with different Sn concentrations deposited on glass substrates.

The thicknesses of films were estimated from these images and are listed in Table 4.2. All films showed similar thicknesses, which were in the range 200-300 nm. The thickness of films depended on the time of spraying and flow rate of solution. The concentration of Sn dopant was not significant for the thickness.

Table 4.2 Thickness of ITO films with different Sn concentrations

Sn concentration (at.%)	Thickness (nm)	
	Value	SD*
0	267.9	13.1
3	204.4	17.4
5	240.7	24.9
7	223.7	26.1
9	294.5	25.8

* SD is standard deviation

4.2.2 Crystal structure

The XRD patterns of ITO films with different Sn concentrations are shown in Figure 4.4. All films were identified as the cubic structure of indium oxide (In_2O_3). The 0 at.% doping film or undoped In_2O_3 film presented the (222) preferred orientation and the intensity of this plane decreased with added Sn concentration. The crystallinity of (400) plane was promoted with the addition of Sn doping and was the preferred orientation with addition of Sn concentration to 5 at.%. This result was consistent with ITO films from other research, which also presented the (400) plane as the preferred orientation [5,6]. As the Sn^{4+} dopant in ITO films substituted into the In^{3+} sites, this behavior caused an increasing of this crystalline phase of these films [77]. When, Sn doping was increased to over 5 at.%, the crystallinity of (400) plane was reduced. This behavior may be caused by Sn doping, which was increased to over the solubility limit of Sn^{4+} ions into the In_2O_3

lattice [78]. The excessive interstitial Sn^{4+} ion formed into a secondary phase as SnO_2, and so this phase leads to a reduction of the crystallinity [78]. The solubility limit of Sn^{4+} ion into In_2O_3 lattice has been reported to be about 4-6 at.% [77-78].

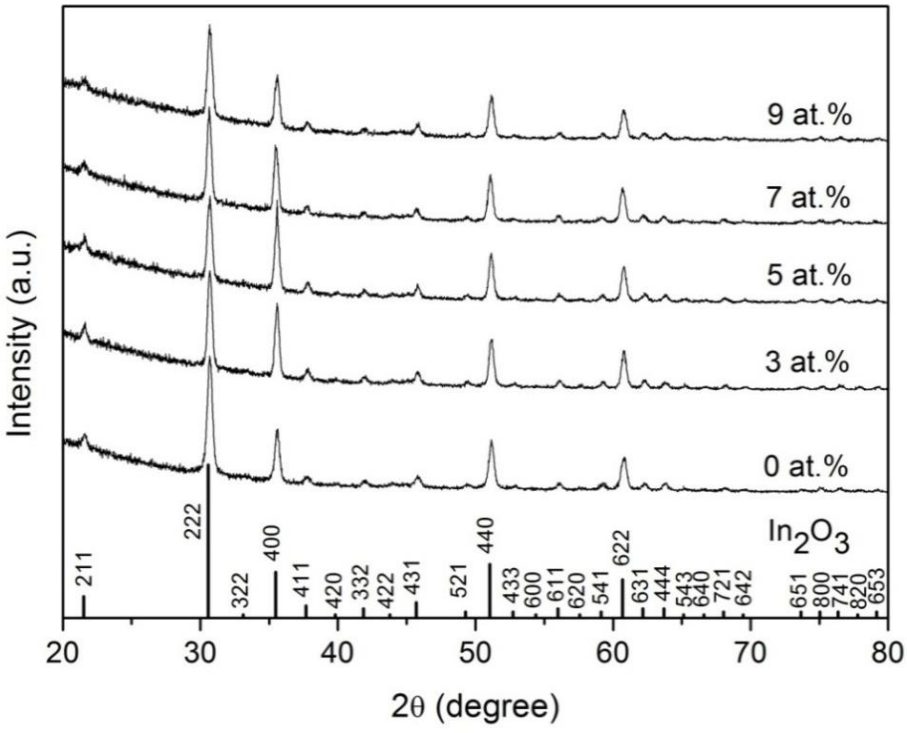

Figure 4.4 The XRD patterns of ITO films with different Sn concentrations.

Table 4.3 Crystallite sizes of (222) and (400) planes of ITO films with different Sn concentrations.

Sn concentrations (at.%)	Crystallite size (nm)	
	hkl (222)	hkl (400)
0	37.45	33.14
3	41.31	36.91
5	39.34	37.59
7	42.73	36.32
9	38.88	33.16

The crystallite sizes of ITO films with different Sn concentrations are listed in Table 4.3. The crystallite sizes of these films can be calculated from FWHM values of the (222) and (400) peaks by equation 3.2 and the FWHM values were obtained from the XRD patterns. The crystallite size variation of the (222) peak was not significant. However, the crystallite size of the (400) plane was found to increase with increasing Sn concentration until 5 at.%. Then, as Sn doping was increased to over 5 at.%, the crystallite size reduced.

4.2.3 Morphology

Surface morphologies of ITO films with different Sn concentrations were investigated by SEM and AFM techniques and are shown in Figures 4.5 and 4.6, respectively. It was observed that the morphology of undoped In_2O_3 films was a loosely packed film with irregular shape and changed to a homogenous film with additional Sn doping. The morphology of the film changed to a cubical shape with additional Sn concentration to 5 at.%. This result agrees with the previous work of *Brinzari et al* [77] where the ITO film was doped with 6 at.% Sn. It could be expected that the Sn^{4+} dopant substituted into the In^{3+} sites and caused the growing of a homogenous film with cubical shapes. Moreover, the XRD pattern of the 6 at.% Sn doped film of this previous work presented the (400) preferred orientation, the same as the XRD results of the 5 at.% Sn doped film in this work. As the Sn doping was increased to more than 5 at.%, the morphology of films changed again to loosely packed films with irregular shape.

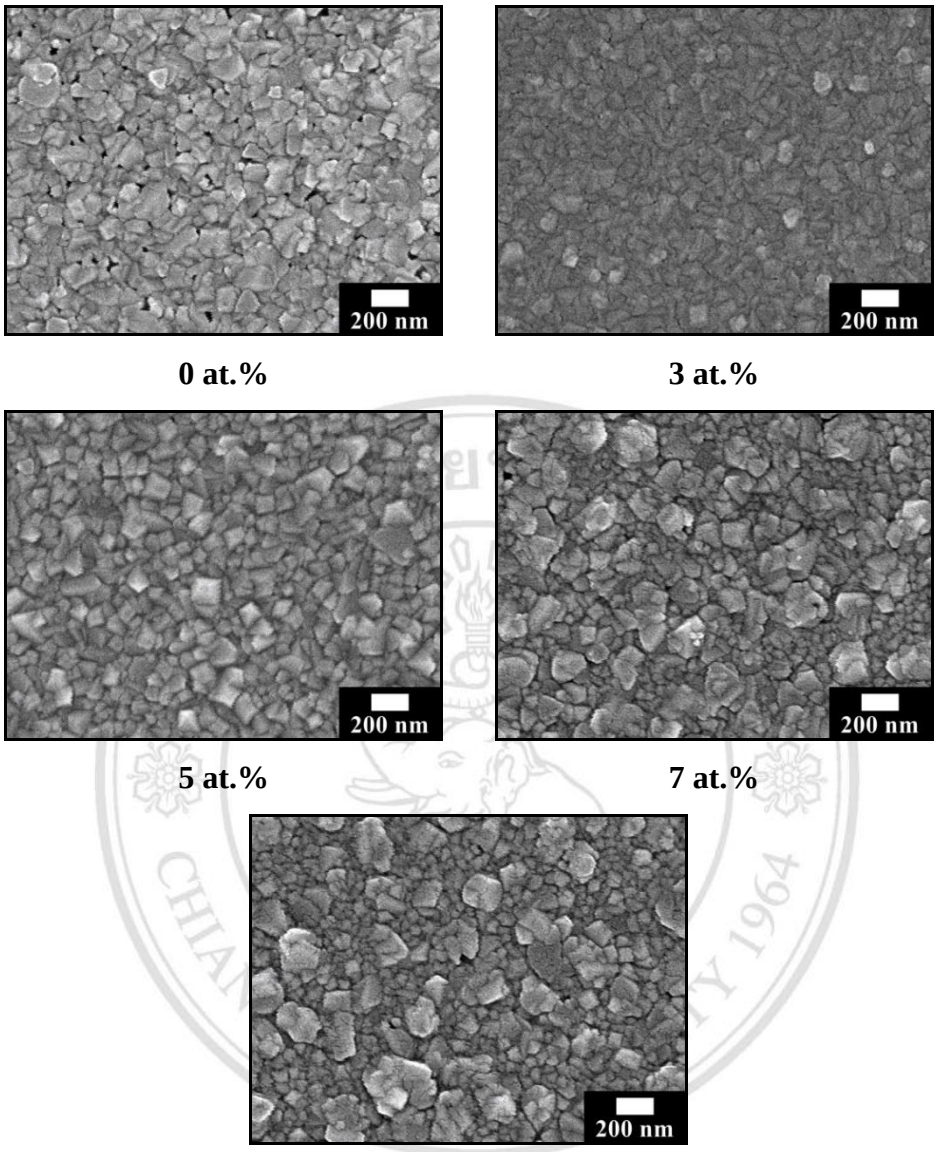

Figure 4.5 SEM images of ITO films with different Sn concentrations.

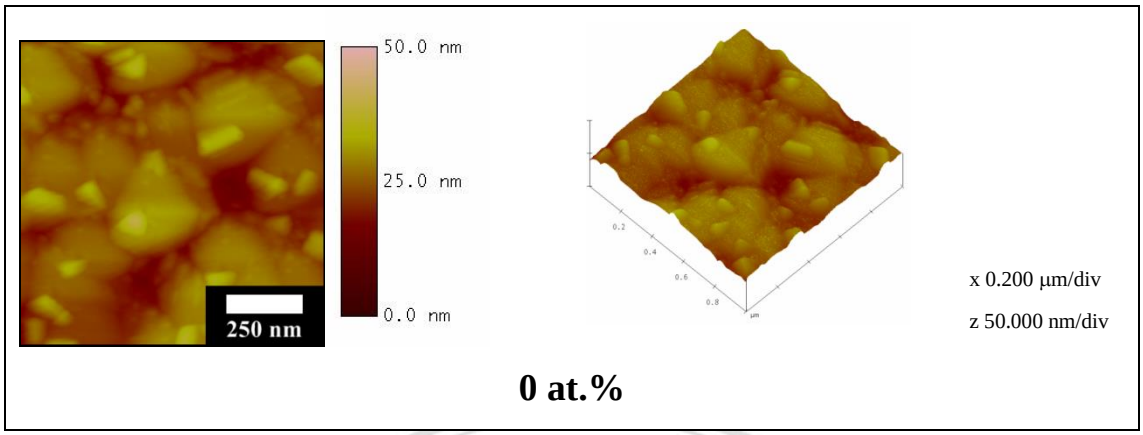

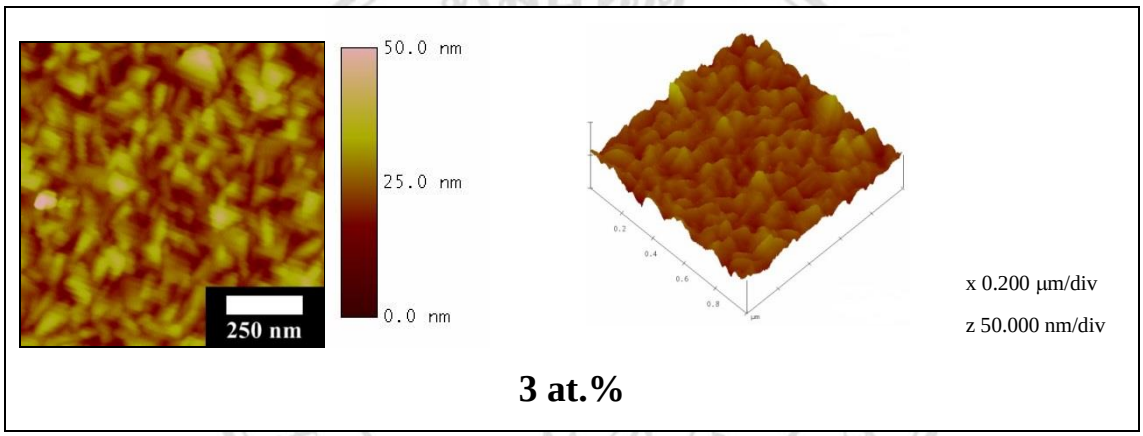

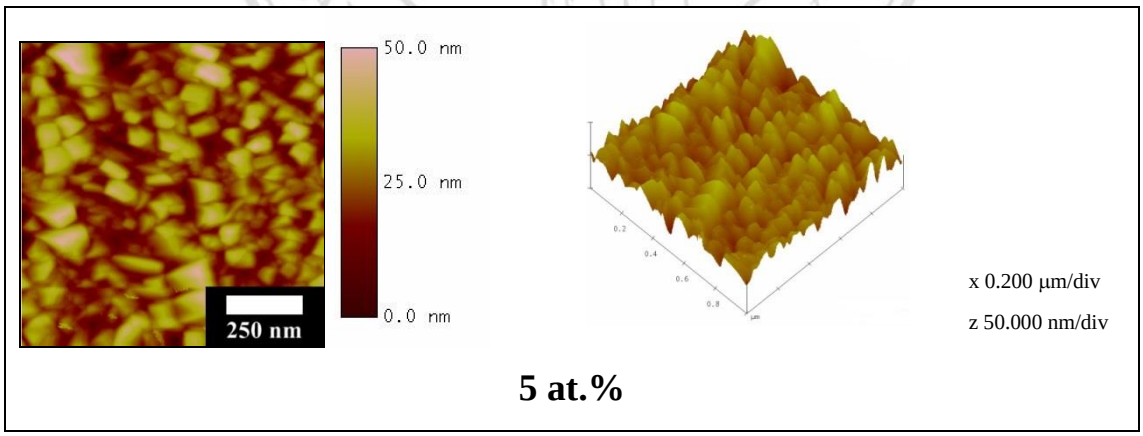

Figure 4.6 AFM images of top ITO films with different Sn concentrations.

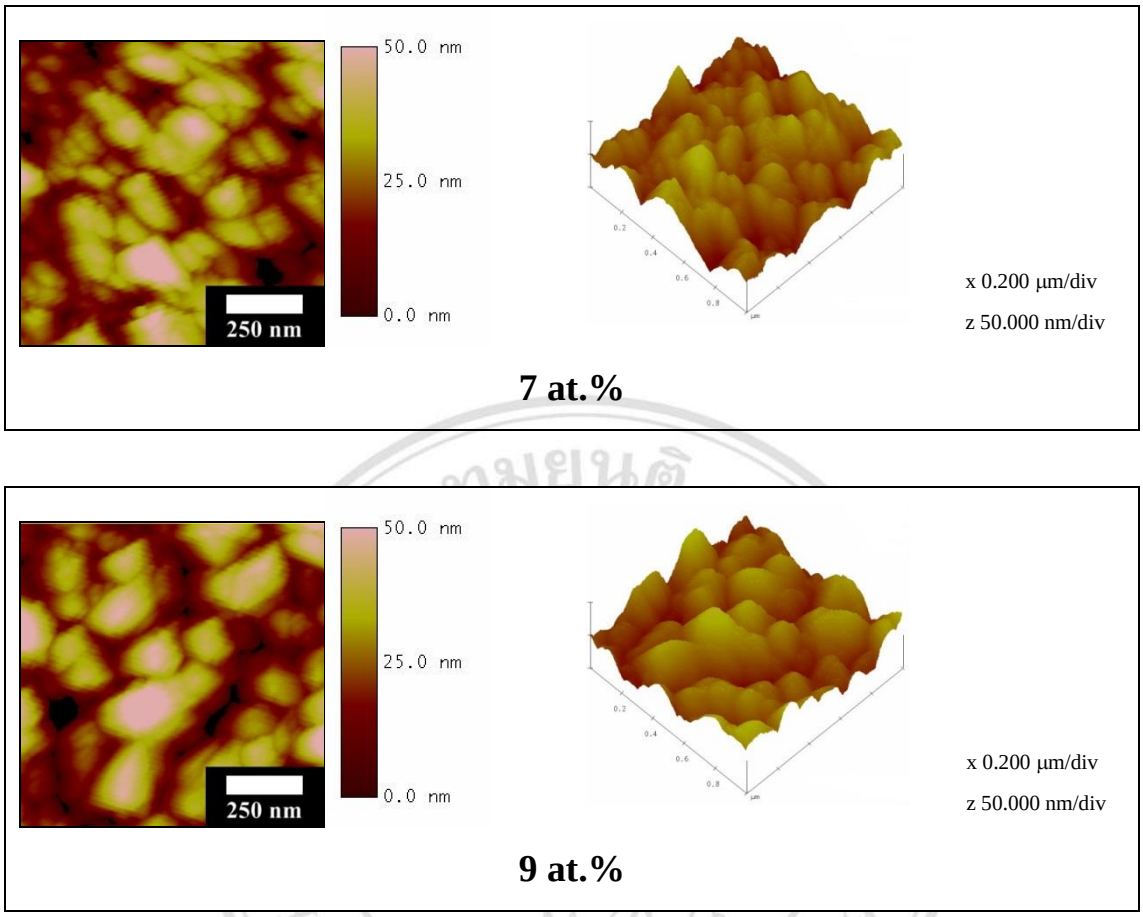

Figure 4.6 AFM images of top ITO films with different Sn concentrations (continued).

The average grain size and surface roughness of films were obtained from these SEM and AFM images, respectively and the trends of these values are shown in Fig. 4.7. The average grain size and surface roughness were found to decrease with doping at 3 at.% Sn and increase with doping to 5 at.% Sn. These behaviors occurred as the Sn^{4+} dopant substituted into the In^{3+} sites [77]. Then, Sn doping was increased to over 5 at.%, the average grain size decreased whereas the surface roughness increased. The increasing of average grain size may be caused by the segregation of a secondary phase, which occurred as the Sn doping was over the limit of solubility into the In_2O_3 lattice. The morphology changed from a homogeneous film to a loosely packed film with doping more than 5 at.% Sn and this result lead to the increasing of surface roughness.

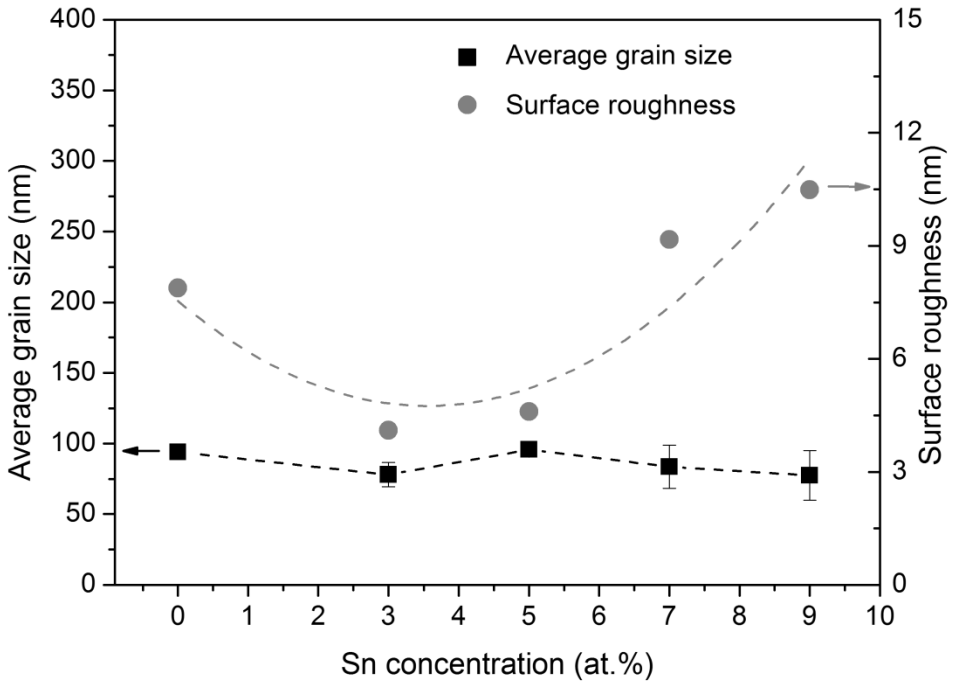

Figure 4.7 Average grain size and surface roughness of ITO films with different Sn concentrations.

4.2.4 Optical properties

The transmittance and absorbance spectra over the wavelength range 300-1000 nm of glass substrate and ITO films with different Sn concentration are shown in Figure 4.8. It was found that the visible range transmittance and absorbance of the glass substrate was about 95% and 0.035. After, coating films on to the glass substrate, the transmittance decreased to about 85% and the absorbance increased to about 0.1 for all conditions. In addition, there was a shift of the absorption edge to higher wavelengths (redshift) with additional Sn doping.

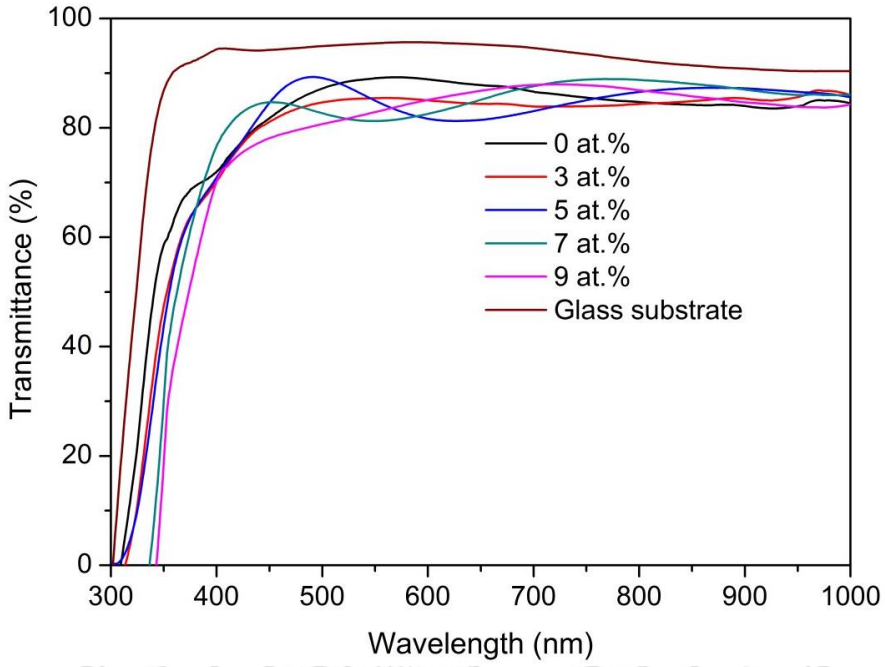

(a) Transmittance

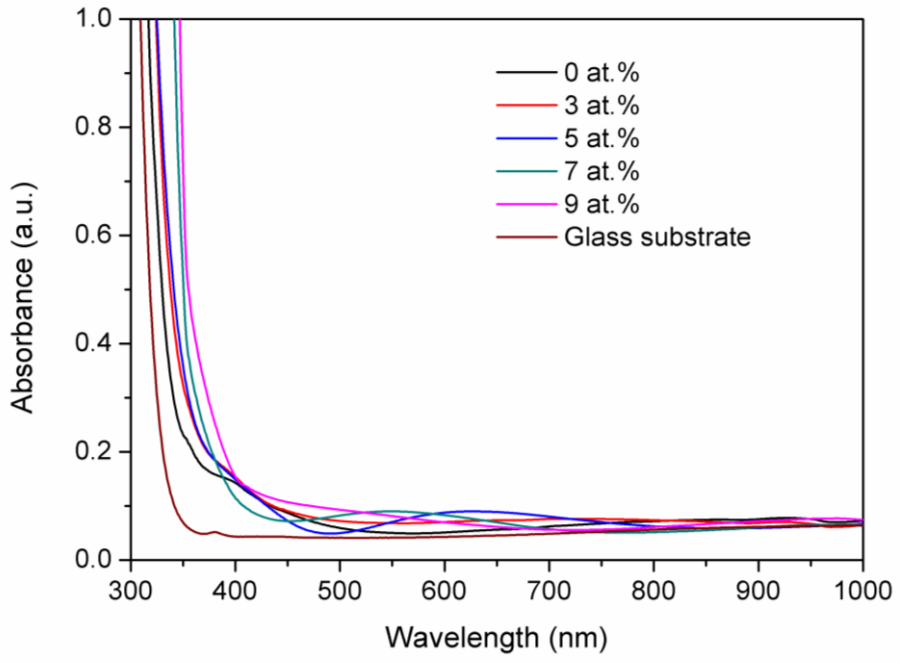

(b) Absorbance

Figure 4.8 Transmittance (a) and absorbance (b) spectra of ITO films with different Sn concentrations.

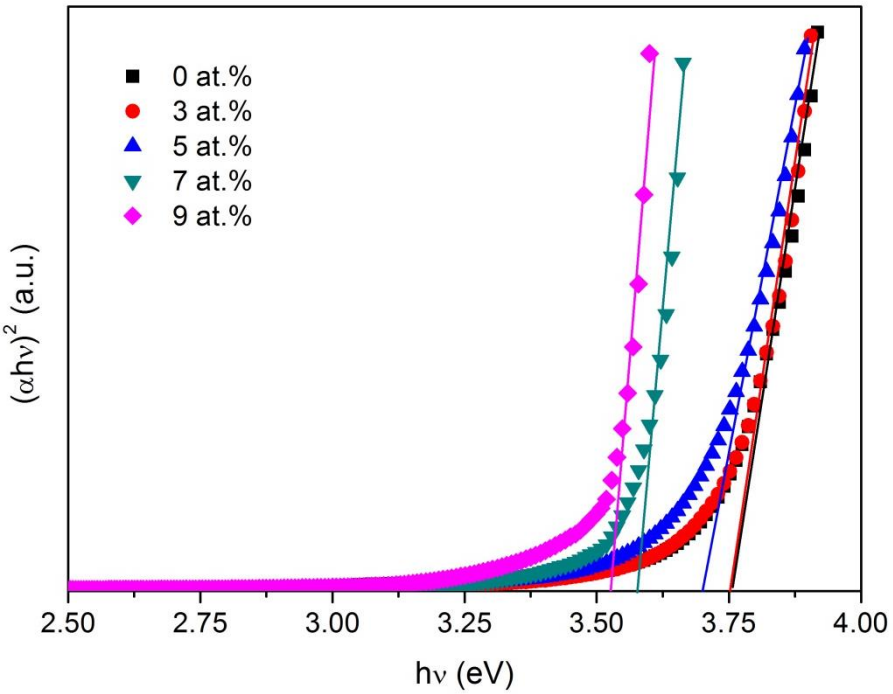

(a) $(\alpha h\nu)^2$ versus $h\nu$ plots

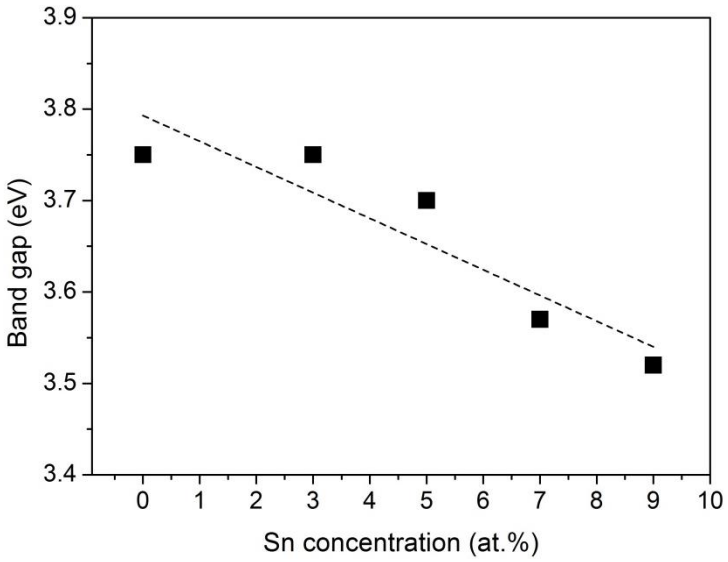

(b) Band gap

Figure 4.9 The $(\alpha h\nu)^2$ versus $h\nu$ plots (a) and the band gap of ITO films with different Sn concentrations.

The band gap of the films was evaluated from the transmittance spectra using Tuac's relationship in equation 3.8 and thickness used in calculations was from Table 4.2. The $(\alpha h\nu)^2$ versus $h\nu$ plots of all films are shown in Figure 4.9 (a) The intercept of $(\alpha h\nu)^2$ on the *x*-axis gave the value of the direct band gap and the band gap of all films as plotted in Figure 4.9 (b). It was observed that the trend of band gap of these films decreased with increasing Sn concentration. This behavior occurred due to many interaction effects of free carrier or/and ionized impurities [66,79]. The free carrier and ionized impurities occurred as the Sn^{4+} dopant substituted into the In^{3+} sites [14,77]. Moreover, redshift behavior occurred due to an increasing of the free carrier density [79].

4.2.5 Electrical properties

The sheet resistance and the resistivity of of ITO films with different Sn concentrations are shown in Figure 4.10. The resistivity was calculated from resistance and thickness of films by equation 3.10 with the thickness as listed in Table 4.2. It was found that the undoped In_2O_3 films showed the highest sheet resistance (~221282 Ω/sq) and resistivity (5.93 Ω.cm). With Sn doped into the In_2O_3 films, the sheet resistance and the resistivity values rapidly decreased to a minimum at 5 at.% Sn doping. The reducing of resistivity of films was caused by Sn^{4+} ion substituting for In^{3+} ions in the In_2O_3 lattice. The difference of the valence electron between In^{3+} and Sn^{4+} results in the donation of a free electron (donor) to the lattice. This donor increased the carrier density of the films [5]. Moreover, the resistivity was found to decrease to a minimum with addition of 5 at.% Sn and increase with further Sn doping. This behavior was caused by the solubility limit of Sn^{4+} into In_2O_3 lattice and has been reported to be about 4-6 at.% [77-78]. Then, the excess Sn formed to a separate phase of SnO_2 and collected at the grain boundary of ITO films and caused the resistivity to increase [5]. These results were consistent with these from other work [5,80]

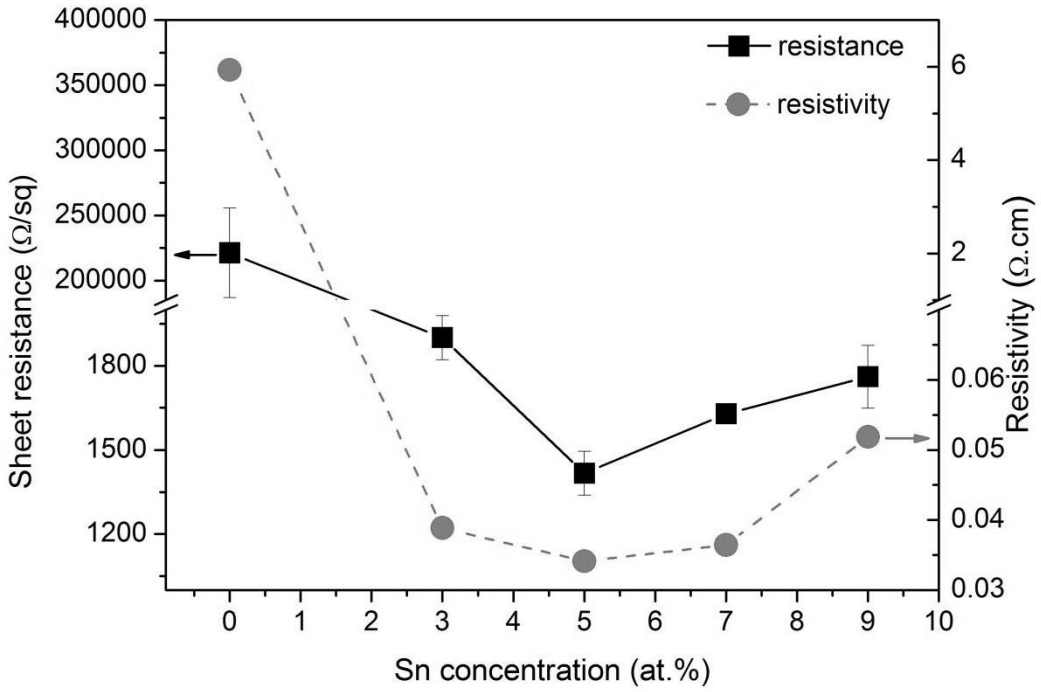

Figure 4.10 The sheet resistance and the resistivity of ITO films with different Sn concentrations.

In the next chapter, the modification of ITO films to ITO/Au/ITO multilayers films is investigated. The ITO film doped with 5 at.% Sn was chosen to be modified to ITO/Au/ITO multilayers films because this ITO film showed the best properties e.g. high transmittance (89%), wide band gap (3.70 eV) and lowest resistivity (1.720 x 10^{-2} Ω.cm).